16th World Congress in Computational Mechanics (WCCM)
21-26 July 2024, Vancouver, Canada
A. Korobenko, M. Laforest, S. Prudhomme, R. Vaziri (Eds)

COUPLING MULTIPLE RESONANCES FOR ENHANCING SOUND TRANSMISSION LOSS OF ACOUSTIC METAMATERIALS

G. Sal-Anglada[1,2], D. Yago[1,2], J. Cante[1,2], J. Oliver[1,3] and D. Roca[1,2,*]

[1] Centre Internacional de Mètodes Numèrics en Enginyeria (CIMNE), 08034 Barcelona, Spain

[2] Universitat Politècnica de Catalunya - BarcelonaTech (UPC), Escola Superior d'Enginyeries Industrial Aeroespacial i Audiovisuals de Terrassa (ESEIAAT), 08222 Terrassa, Spain

[3] Universitat Politècnica de Catalunya - BarcelonaTech (UPC), Escola Tècnica Superior d'Enginyers de Camins, Canals i Ports de Barcelona (ETSECCPB), 08034 Barcelona, Spain

[*] Corresponding author: david.roca.cazorla@upc.edu

Key words: Acoustic metamaterials, Sound transmission loss, Coupled resonances, Machine Learning, Computational design.

Abstract. Recent developments in acoustic metamaterials have been focused on broadening the attenuating bandwidth features towards lower frequency ranges, well below 1000 Hz, as well as tackling manufacturing issues. In this context, a multi-resonant layered acoustic metamaterial (MLAM) was proposed as a practical realization for addressing both challenges. The MLAM's layered-based design makes it amenable to large-scale manufacturing and the periodic features of each layer enable the application of computational homogenization models to characterize the sound transmission loss (STL) response. Combining these models with optimization techniques allows to determine realistic MLAM designs that trigger multiple resonances in broad frequency ranges. By exploiting coupling mechanisms these resonances translate into multiple STL peaks that produce a broadband continuous frequency range of attenuation, i.e., without transmission peaks in-between. In this work, the proposed computational homogenization model is presented and applied to the design of different MLAM configurations. The goal is to assess the influence of the number of coupled resonating layers in the STL response of the whole MLAM panel, in terms of increasing the attenuation intensity and the effective frequency bandwidth. The results demonstrate the STL enhancements features obtained from exploiting coupling mechanisms, compared to other acoustic metamaterial configurations based on local resonance phenomena. In this context, the proposed MLAM technology exhibits a great potential to provide an efficient, easy-to-manufacture solution to the sound insulation problem at low frequency ranges.

1 INTRODUCTION

The study of acoustic metamaterials has surged due to their promise of exceptional properties across various applications, particularly in soundproofing within specific frequency ranges without increasing mass [1]. These materials leverage internal resonances within their structures to create frequency band gaps, making them efficient in sound manipulation [2]. Their capability to trigger resonances at sub-wavelength scales has driven their popularity for applications below 1000 Hz, where traditional materials require thick or dense configurations.

Early designs combined different material components within unit cells, such as dense inclusions in soft matrices, and membrane-based configurations targeted lower frequencies but with compromised load-bearing capabilities. More recent designs focus on geometric features to trigger internal resonances, though challenges in manufacturing scalability remain [3]. Despite these advancements, many local resonance-based metamaterials are constrained by narrow frequency ranges. Coupled resonances, as introduced by Roca and Hussein [4] and further studied in Ref. [5], have shown potential for broadband attenuation.

Layered-based acoustic metamaterials, inspired by conventional double-leaf walls, have been proposed to address manufacturing challenges [6]. These designs incorporate multiple resonating inclusions to create a series of attenuation peaks in the sound transmission loss (STL) response. The main issue in such designs lies in the presence of strong dips between STL peaks, which can be mitigated by exploiting coupled resonances. A multiresonant layered acoustic metamaterial (MLAM) capable of a double-peak STL response exploiting the coupled resonance phenomenon was proposed in Ref. [7], and enhanced with a zero-stiffness device to trigger a third coupled peak [8].

To improve the performance and scalability of the MLAM structure, this article proposes an extension capable of triggering multiple coupled peaks. We analyze the n-peak coupled resonance phenomenon, its STL enhancement capabilities, and limitations. Our approach to designing metamaterial panels based on this concept, referred to as n-MLAM, involves a three-step strategy: (1) layer-by-layer homogenization to build a database of effective properties, (2) integration of Neural Networks (NN) for efficient property interpolation, and (3) using a genetic algorithm (GA) to optimize the resulting solution. This method, inspired by Ref. [9], addresses the computational cost and accuracy limitations of previous interpolation functions [10]. The benefits of ML in optimizing metamaterial structures have been discussed in various studies [11], highlighting its potential in expanding the design space and finding new optimal solutions for sound insulation applications. The results demonstrate how the n-MLAM concept enhances effective attenuation bandwidth and/or level, emphasizing its potential for soundproofing and noise reduction applications.

2 ANALYTICAL MODEL FOR MULTIPLE COUPLED RESONANCES

The analytical foundation of our study is demonstrated by the general spring-mass system depicted in Figure 1. The model contains a collection of n distinct mass-in-mass units interconnected with each other through springs of stiffness K_{c}. Each of these units consists of an

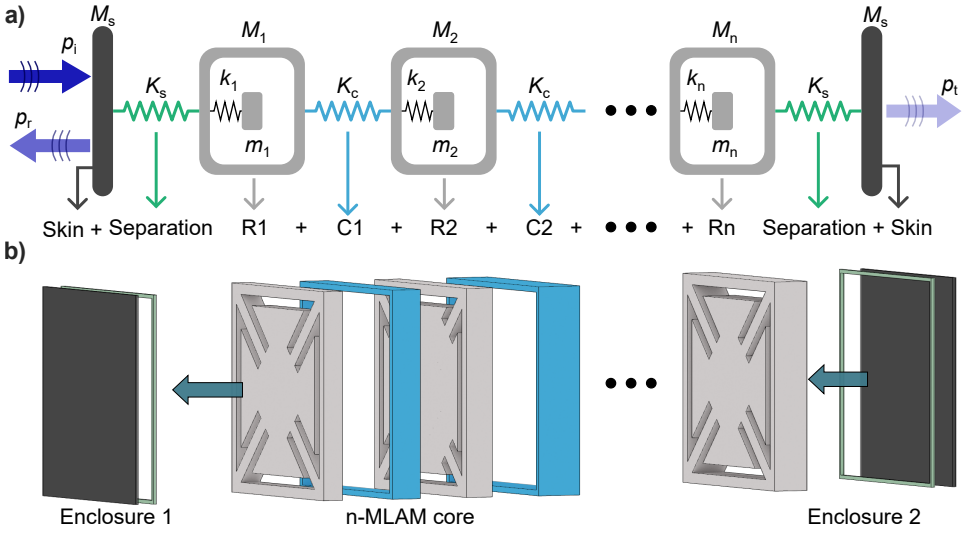

Figure 1: (a) General spring-mass model for the n-MLAM design used in the analytical analysis. (b) Layers comprised in a n-MLAM panel structure. The core is composed of a collection of n resonating layers (represented by mass-in-mass units in the equivalent spring-mass model) interconnected by connecting layers in-between. The core is enclosed by skin and separating layers at both sides.

external mass, M_i, and an internal mass, m_i, attached by a spring of stiffness k_i. In turn, the mass-in-mass chain is attached by springs of stiffness K_s to outer masses, M_s, at both ends. The first of these is excited by an incident and a reflected acoustic wave, with amplitudes p_i and p_r,

$$p_\mathrm{in} = (p_\mathrm{i} e^{\mathrm{i}\kappa x} + p_\mathrm{r} e^{-\mathrm{i}\kappa x}) e^{-\mathrm{i}\omega t}, \tag{1}$$

and the latter is subjected to a transmitted wave, with amplitude p_t,

$$p_\mathrm{out} = p_\mathrm{t} e^{\mathrm{i}(\kappa x - \omega t)}, \tag{2}$$

where ω is the frequency, and $\kappa = \omega / c_\mathrm{a}$ is the corresponding wavenumber ($c_\mathrm{a} = 340$ m/s referring to the speed of sound in air). To impose displacements compatibility, Euler's equation is used to relate the acceleration with the pressure gradient

$$\rho_\mathrm{a} \ddot{u} = -\frac{dp}{dx}, \tag{3}$$

where $\rho_\mathrm{a} = 1.25$ kg/m^3 is the air's density, and u is the displacement ($\ddot{u}$ refers to the acceleration). Denoting u_in and u_out the displacements of the outer masses, applying Eq. (3) with Eqs. (1) and (2) in the frequency domain yields

$$u_\mathrm{in} = \frac{\mathrm{i}}{\rho_\mathrm{a} c_\mathrm{a} \omega} (p_\mathrm{i} e^{\mathrm{i}\kappa x} - p_\mathrm{r} e^{-\mathrm{i}\kappa x}) e^{-\mathrm{i}\omega t}, \tag{4}$$

$$u_\mathrm{out} = \frac{\mathrm{i}}{\rho_\mathrm{a} c_\mathrm{a} \omega} p_\mathrm{t} e^{\mathrm{i}(\kappa x - \omega t)}. \tag{5}$$

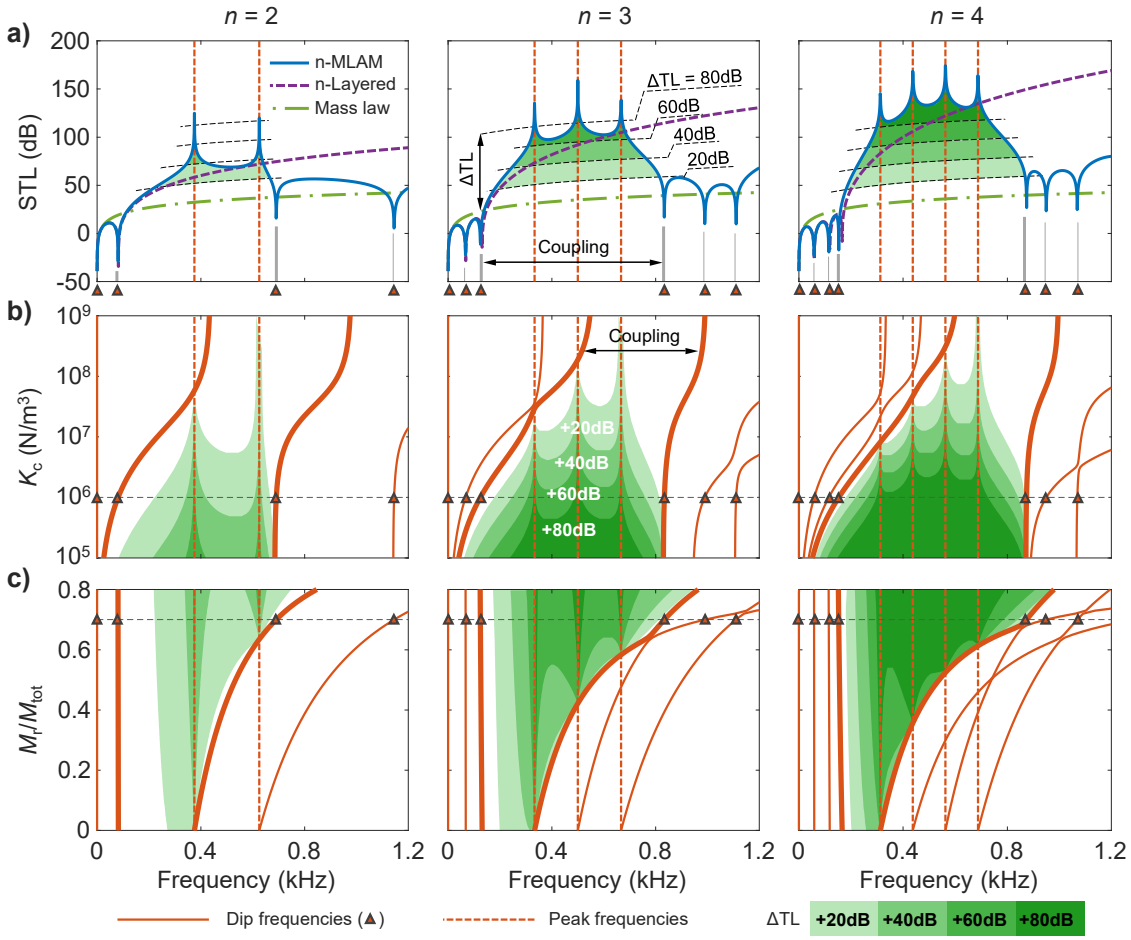

Figure 2: (a) STL curves (solid blue lines) for the reference spring-mass models of the 2-MLAM (left), 3-MLAM (centre) and 4-MLAM (right) cases. The STL curves corresponding to the mass law for 15 kg/m^2 (dash-dotted green lines) and to the equivalent spring-mass model without resonators (dashed purple lines) are also shown, as a reference. (b) Change in the STL dip frequencies (solid orange lines), as a function of the connecting springs' stiffness. (c) Change in the dip frequencies as a function of the resonators' mass fraction. Thick orange lines mark the dip frequencies that determine the bounds of the coupling window. The horizontal dashed black lines indicate the reference case, for which the corresponding STL is shown in (a).

For a given frequency—and imposing Eqs. (4) and (5) as boundary conditions and Eqs. (1) and (2) as external forces—the equations of motion for the spring-mass system can be solved in terms of the amplitude of the incident wave, allowing us to get the transmission coefficient of the system, $T = p_t/p_i$. Then, the sound transmission loss (in decibels) can be obtained as

$$\mathrm{STL}(\omega) = -20 \log_{10} |T(\omega)|. \tag{6}$$

To show the effects of increasing the number of resonators in the coupled resonances mechanisms, the STL response for cases with $n = 2$, 3 and 4 resonators has been studied. As a reference, a total surface mass of $M_{tot} = 15$ kg/m^2 has been considered. A 20% fraction of the total

mass has been distributed equally among the outer masses, so $M_{\mathrm{s}} = 0.1M_{\mathrm{tot}}$, and a 70% fraction has been distributed equally among the internal resonators, so $m_i = M_{\mathrm{r}}/n$ with $M_{\mathrm{r}} = 0.7M_{\mathrm{tot}}$. The remaining 10% has been distributed equally among the external masses in the mass-in-mass units, so $M_i = (0.8M_{\mathrm{tot}} - M_{\mathrm{r}})/n$. A stiffness per unit of area of $K_{\mathrm{s}} = 10^{12}$ N/m^3 has been considered for the outer springs and $K_{\mathrm{c}} = 10^6$ N/m^3 for the interconnecting springs between the mass-in-mass units. The stiffness of the interconnecting springs is much smaller to allow effective coupling. As for the internal resonators' stiffness, it has been adjusted to trigger resonances at evenly spaced frequencies in the 250–750 Hz range for each case. Notice that all values have been normalized by a unit cross-sectional area, since the one-dimensional nature of the system makes the STL response to be independent of it. These values have been chosen to obtain similar STL curves—in terms of frequency range and order of magnitude of the intensity levels—to those for the actual n-MLAM panels described in the Sections 3 and 4.

The STL responses for the 2, 3, and 4-MLAM cases are shown in Figure 2(a), along with the mass law curve for 15 kg/m^2 and the STL response of an equivalent spring-mass system without internal resonators. All cases show significant improvements in attenuation level compared to the mass law, with higher ΔTL as the number of resonators increases. Most enhancement is due to the coupling mechanism, but internal resonators further improve attenuation, especially at lower frequencies, extending the effective bandwidth.

To understand the benefits and limitations of multi-coupling resonances, two parametric studies were performed. The first varied the stiffness of the connecting springs, K_{c}, from 10^6 to 10^9 N/m^3. The second varied the mass fraction of resonators from 0% to 80%. Results are shown in Figures 2(b) and 2(c). The STL dip frequencies, $f_i^{(\mathrm{d})}$, change with these parameters, but a coupling window can be identified by $f_n^{(\mathrm{d})}$ and $f_{n+1}^{(\mathrm{d})}$ frequencies. Reducing spring stiffness enlarges the coupling window, leading to higher attenuation levels. Concentrating mass in internal resonators increases STL levels and effective bandwidth. Results show that increasing the number of resonators generally improve the STL response (both in terms of attenuation levels achieved and effective bandwidth), but at the expense of requiring more compliant springs—which might increase layer thickness and reduce load-bearing capabilities.

3 DESIGN STRATEGY OF n-MLAM

The n-MLAM panel comprises various layers with constant cross-sections defined by a specific pattern repeated periodically across the in-plane directions, as depicted in Figure 1(b). The coupled resonances are achieved by the resonating and connecting layers forming the core structure of the n-MLAM panel. The unit cell of the resonating layers includes an external frame linked to an inner flower-like resonant element, enabling oscillation at a specified resonance frequency. The connecting layers, consisting of an outer frame with thickness h, provide structural connections and facilitate acoustic coupling. Additional separation and skin layers are added at both ends to enclose and protect the structure. This layered configuration allows n-MLAM panels to be fabricated using established techniques, such as lamination, die-cutting, and final stacking and bonding. These methods are compatible with mass production, reducing manufacturing costs.

The n-MLAM panel design strategy is anchored in three pivotal techniques: (1) a one-dimensional homogenization of individual layers (i.e., layer-by-layer homogenization), yielding a 1D rod reduced model that represents the macroscopic intricacies of the acoustic insulating material, (2) the establishment of a surrogate model based on neural networks to predict and estimate the effective properties derived from homogenization in a continuous expression, and (3) the optimization of layer topology within the n-MLAM panel via a Genetic Algorithm that seamlessly integrates the prior two techniques.The approach aims to identify optimal n-MLAM configurations that enhance sound transmission attenuation by coupling all resonators. This is achieved through the synergy of homogenization and neural networks, enabling efficient estimation of the acoustic response from geometric parameters. With this objective in mind, layer databases are created to train deep-learning surrogate models, which are then used in the optimization algorithm. The general design strategy is depicted in Figure 3.

Figure 3-a provides a detailed breakdown of the geometrical parameters. A standard polyamide material (density $\rho = 1050$ kg/m^3, Young's modulus $E = 1650$ MPa, Poisson's ratio $\nu = 0.4$) is used for the skin, separating, and resonating layers, while a rubber-like material (density $\rho = 1060$ kg/m^3, Young's modulus $E = 0.15$ MPa, Poisson's ratio $\nu = 0.47$) is used for the connecting layers.

3.1 Layer-by-layer homogenization

To accurately assess the STL response of the n-MLAM during the optimization process, the homogenization model proposed in Sal-Anglada et al. [9] is employed. The foundation of this model lies on a general multiscale homogenization framework that capitalizes on the assumption of distinct scales in the material structure [12]. These scales correspond to the macroscale, where apparent wave-propagating behavior occurs, and the microscale, where the internal structure triggers local resonance effects. To link both scales, the following kinematic relation is imposed at each layer j in the MLAM structure:

$$\mathbf{u}_\mu^{(j)} = \begin{Bmatrix} u_\mu^{(j)} \\ v_\mu^{(j)} \\ w_\mu^{(j)} \end{Bmatrix} = \begin{Bmatrix} 1 \\ 0 \\ 0 \end{Bmatrix} \bar{u}^{(j)} + \begin{Bmatrix} x'^{(j)} - x_0'^{(j)} \\ 0 \\ 0 \end{Bmatrix} \varepsilon^{(j)} + \begin{Bmatrix} \tilde{u}_\mu^{(j)} \\ \tilde{v}_\mu^{(j)} \\ \tilde{w}_\mu^{(j)} \end{Bmatrix} \tag{7}$$

where $\mathbf{u}_\mu^{(j)} = (u_\mu^{(j)}, v_\mu^{(j)}, w_\mu^{(j)})$ are the displacement field components in the microscale (referred to by the sub-index μ), $\bar{u}^{(j)}$ is an effective uniform (rigid body) translation of the layer in the x-direction, $\varepsilon^{(j)}$ is a uniform stretch of the layer in the x-direction, $x_0'^{(j)}$ is the middle x-coordinate of the layer thickness, and $\tilde{\mathbf{u}}_\mu = (\tilde{u}_\mu^{(j)}, \tilde{v}_\mu^{(j)}, \tilde{w}_\mu^{(j)})$ are the microfluctuations field components. The microfluctuation field vanishes at the interface between layers—to guarantee displacement compatibility conditions—and satisfies periodic boundary conditions in the in-plane directions—to simulate an infinite extension of the layer's unit cell pattern.

The reaction to the uniform displacement and stretch imposed by Eq. (7) yield effective values of an inertial force density and a normal stress—in the thickness direction of the layer—from which a set of macroscopic properties can be derived. In particular, effective density $\rho_{\text{eff}}^{(j)}$

and elastic modulus $E_{\text{eff}}^{(j)}$ are obtained as measures of the mass and stiffness of the layer. The local resonance effects triggered in the resonating layers are also captured by the homogenization model by means of the derivation of an equivalent internal mass, $\tilde{m}^{(j)}$, and stiffness, $\tilde{k}^{(j)}$, obtained from the corresponding structural mode, associated to the resonance frequency $\tilde{\omega}^{(j)}$. Specific details on the derivation of these effective properties are given in Ref. [9]. As a result of this homogenization process applied to each layer, one is capable of representing the response of the layer to waves propagating in the normal direction through an equivalent structural rod model—with a spring-mass system attached, in the case of the resonating layers—with the aforementioned effective properties, as depicted in Figure 3-a. This simplified one-dimensional model can then be used to accurately evaluate the STL response of a n-MLAM structure, regardless of the number of layers involved, extremely fast.

3.2 Neural Networks

Integrating machine learning into acoustic metamaterial design significantly advances over conventional techniques, particularly in database creation and computational costs [9]. Neural network-based models efficiently map the design space using random sampling strategies (e.g., Latin Hypercube Sampling, Sobol sequence), eliminating the need for rigid grid approaches and reducing the number of data samples required. Consequently, NN-based models handle more design variables without increasing computational costs, enabling exploration of more complex topologies and potentially yielding superior optimal outcomes.

A neural network-based surrogate model is created for each layer type within the n-MLAM panel to map topological designs to effective properties in the 1D homogenized model (Figure 3-a). A comprehensive database is built through homogenization, assessing effective properties for various topological configurations. The surrogate models are divided into two sets: (a) skin, separating, and connecting layers, and (b) resonating layers. For the first group, the design relies on layer thickness h, while resonating layers are characterized by h, w_{a}, d_{a}, and w_2. The design space is sampled using a Sobol sequence, with 40 samples for simpler layers and 7500 for resonating layers. Relevant variables range as follows: $h^{(\text{skin})}, h^{(\text{separating})} \in [0.5, 10]$ mm; $h^{(\text{connecting})} \in [0.5, 25]$ mm; $h^{(\text{res})} \in [1, 10]$ mm; $w_{\text{a}}^{(\text{res})} \in [1, 8]$ mm; $d_{\text{a}}^{(\text{res})} \in [5, 30]$ mm; $w_2^{(\text{res})} \in [1, 12]$ mm; with other parameters set to $a = 60$ mm, $w_1 = 1$ mm, $w_f = 1.5$ mm, and $w_c =$ 1mm.

A fully connected feedforward neural network (FFNN) is proposed for each layer group to estimate the effective properties for acoustic characterization. Two independent neural networks model the properties of resonating layers: (a) unit cell properties (ρ_{eff} and E_{eff}), and (b) internal resonator properties ($\tilde{k}$, $\tilde{m}$, and $\tilde{\omega}$). Hyperparameters, including hidden layers and neurons, are determined through Bayesian optimization, resulting in architectures $\mathcal{N}^5[58, 31, 30, 12, 12]$ for external parameters and $\mathcal{N}^5[60, 33, 7, 30, 16]$ for internal parameters. Simpler layers use a constant 4-layer architecture with 30 neurons each (i.e., $\mathcal{N}^4[30, 30, 30, 30]$). Each hidden layer uses a hyperbolic tangent sigmoid activation function, and the output layer uses a linear activation function. The models are trained in Matlab using a Bayesian regularization algorithm, with the database split into training (70%), testing (15%), and validation (15%) sets.

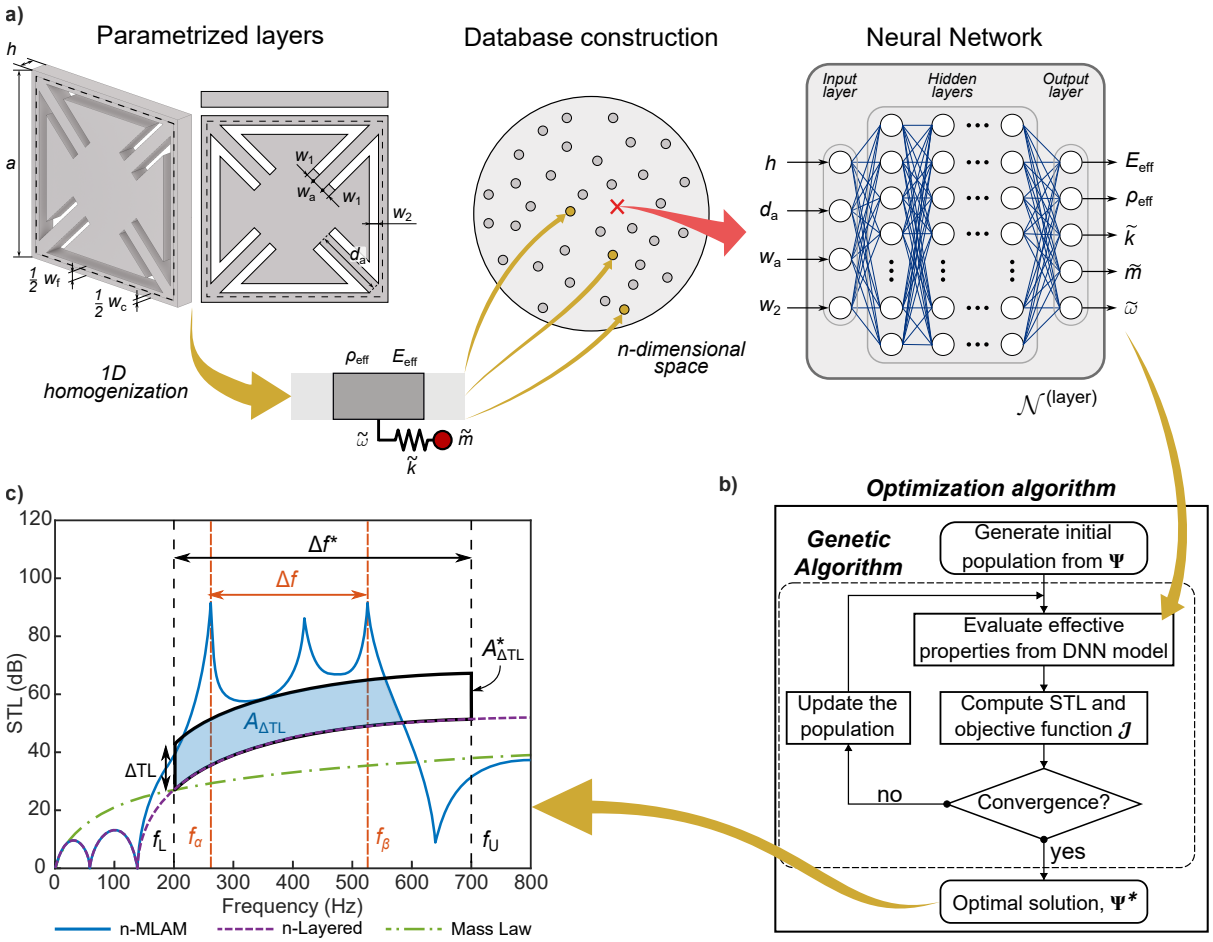

Figure 3: (a) Schematic of the ML model for predicting the effective properties of each layer within the n-MLAM panel, involving a comprehensive database of geometric parameters and corresponding effective properties derived from the homogenization framework. A surrogate DNN model is trained on this dataset, with the design space systematically mapped using a Sobol's sequence. (b) The optimization algorithm uses a genetic algorithm to explore optimal geometrical values, represented by the parameter set $\boldsymbol{\Psi}$, leveraging the surrogate model for efficient STL computation, providing almost immediately the objective function $\mathcal{J}$ for each configuration. (c) Example STL response for a 3-MLAM. It compares the n-MLAM with a homogeneous material solution, using the same connecting layers for a fair comparison, and also presents the mass law as a reference. Optimization focuses on maximizing the area $A^*_{\Delta\text{TL}}$ (shaded in blue) inside the attenuation window (outlined by the bold black line), defined by a target bandwidth Δf^* and STL improvement ΔTL.

This surrogate Deep Neural Network (DNN) model accurately estimates effective properties with a computational cost nearly independent of the number of n-MLAM panel layers. This cost reduction facilitates seamless integration with optimization techniques, enabling efficient assessment of optimal n-MLAM panel designs compared to resource-intensive 3D analyses. This reduction is crucial for the optimization strategy, as conventional parametric-based approaches would be unaffordable, narrowing the design space and limiting potential solutions.

3.3 Optimization with Genetic Algorithm

The optimization problem aims to identify the optimal geometrical parameters for each layer within the n-MLAM panel to maximize sound attenuation across a specified frequency range, relative to a homogeneous material of equivalent mass. The parameter set $\mathbf{\Psi}$ includes layer thicknesses (for connecting and resonating layers) and resonating layer parameters (w_{a}, d_{a}, and w_2) (Figure 3-a). A genetic algorithm (Figure 3-b) integrates the previously discussed techniques, efficiently obtaining optimized solutions by leveraging pre-trained NN-based surrogate models and homogenization of the n-MLAM panel. Despite the increase in parameters with more resonating layers ($4n + (n - 1)$ design variables), the use of surrogate models and 1D homogenization expedites STL evaluation, minimizing the impact on computational cost.

In general, the main objective is to maximize the sound attenuation window $A_{\Delta\mathrm{TL}}$ in the interval $[f_{\mathrm{L}}, f_{\mathrm{U}}]$, while also optimizing the total attenuation bandwidth Δf (Figure 3-c). The STL increase is considered relative to an n-layered homogeneous configuration to focus on the effects of adding resonating elements. The objective function $\mathcal{J}$, based on geometrical parameters $\mathbf{\Psi}$, is:

$$\mathcal{J}(\mathbf{\Psi}) = \frac{A_{\Delta\mathrm{TL}}(\mathbf{\Psi})}{A^*_{\Delta\mathrm{TL}}} + \zeta \log\left(\frac{\Delta f(\mathbf{\Psi})}{\Delta f^*}\right) \tag{8}$$

where $A^*_{\Delta\mathrm{TL}}$ is the target attenuation area, and Δf^* is the target frequency range. The parameter $\zeta \geq 0$ balances the influence of attenuation bandwidth. Additional constraints ensure resonant peak coupling, impose upper bounds on thickness and surface density, address manufacturability and integrity, and optimize within the surrogate model's design space. The size optimization is implemented in Matlab using the *ga* function with a population of 300, heuristic-type crossover ratio of 1.5, and a crossover fraction of 0.6. A constrained optimization using the *fmincon* function is then performed to refine the solution.

4 RESULTS

In the following, a size optimization is performed for various n-MLAM panels using the strategy outlined in the preceding section. The analysis particularly targets optimizations for panels featuring 2, 3, and 4 resonating layers, resulting in optimized topologies exhibiting up to 4 coupled peaks in the STL response. The optimization scenarios, guided by the objective function (8), involve either (1) maximizing the attenuation bandwidth for a specified target attenuation level relative to the homogeneous insulating material (e.g., $\Delta\mathrm{TL} = 20$ dB), or (2) maximizing the attenuation level within a limited attenuation bandwidth. The choice between these criteria profoundly influences the optimal configuration, contingent on the specific target application.

For the numerical examples, the optimization of n-MLAM panels with varying numbers of resonating layers is undertaken while adhering to a consistent surface density of 15 kg/m^2 and a maximum panel thickness of 40 mm. Additionally, an extra numerical constraint is introduced to ensure that the dip closer to the first resonance frequency is obtained at around 200 Hz.

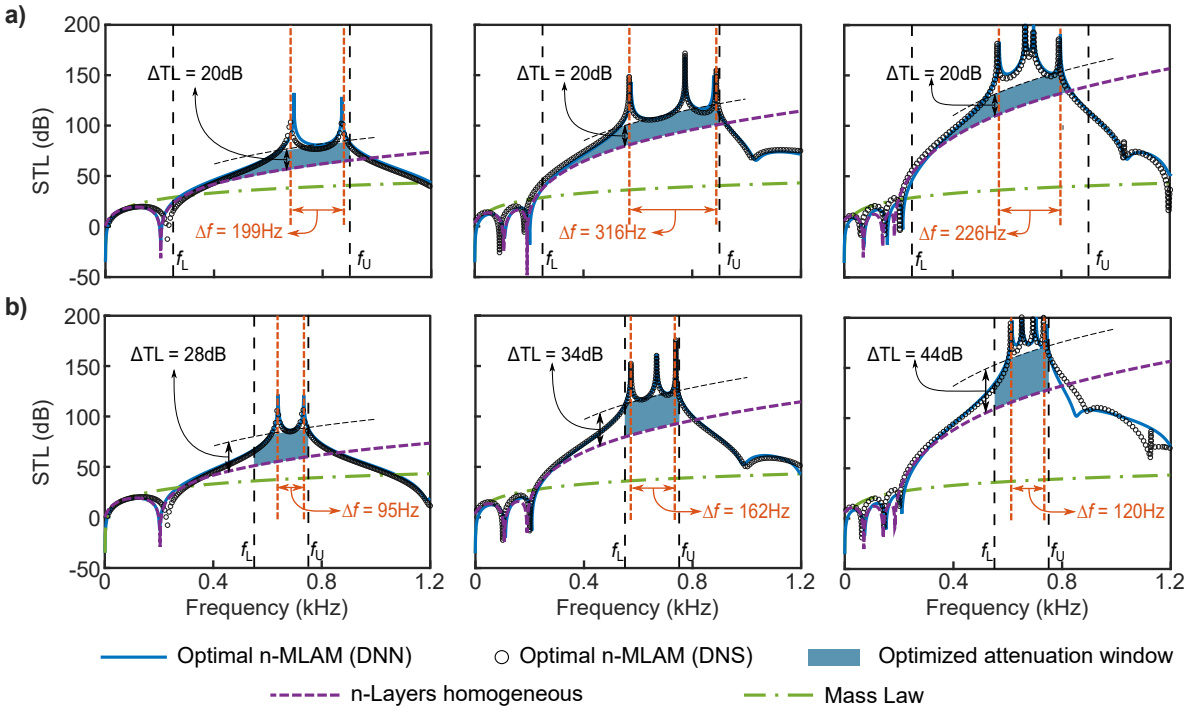

Figure 4: STL response and outcomes for different n-MLAM panel configurations under two optimization scenarios: (a) bandwidth maximization (see Section 4.1), and (b) attenuation level maximization (see Section 4.2). Each column corresponds to cases with 2, 3, and 4 peaks. All solutions depicted in the figure maintain the same surface density of 15 kg/m^2. The figure depicts the optimal n-MLAM interpolated with neural networks (solid blue lines), the STL obtained for the same configuration validated by a direct numerical simulation (black 'o' shaped marks), the equivalent n-layered homogeneous case (dashed purple lines), and the mass law (dash-dotted green lines). Shaded areas highlight the optimized attenuation windows in each case.

While this constraint does not guarantee a direct comparison between n-MLAM panels with different numbers of resonating layers, it establishes a reference STL response for panels with the same number of resonating layers, thereby facilitating comparative analysis across different scenarios.

The following discussion delves into the results of the topology optimizations in both scenarios (shown in Figure 4), comparing STL responses of the optimized n-MLAM panels with those obtained from direct numerical simulations. These show good agreement, validating both the homogenization model employed and the DNN-based interpolation. Furthermore, the STL responses of the mass law for the reference surface density and that for the homogeneous acoustic insulating material are presented. This latter configuration exhibits a STL response with n dips, allowing the tuning of the last dip frequency to 200 Hz.

4.1 Maximize attenuation bandwidth

The objective in this scenario is to maximize the attenuation bandwidth Δf in the STL response, achieving a 20 dB improvement compared to homogeneous n-layered material within the 250 Hz to 900 Hz range ($\zeta = 0.4$). Results, displayed in Figure 4(a) for 2, 3, and 4 resonating layers, reveal a notable increase in attenuation levels as the number of resonating layers increases, reaching up to 200 dB for panels with 4 layers. Transitioning from a 2-MLAM panel to a 3-MLAM panel shows a bandwidth increase of over 100 Hz with a slight rise in attenuation level. However, adding an additional resonating layer results primarily in enhanced attenuation, likely due to the challenge of achieving an STL response with 4 coupled peaks while meeting other optimization constraints. Relaxing certain constraints, such as surface density or maximum panel thickness, may allow for further improvements.

4.2 Maximize attenuation level

In this scenario, the focus is on maximizing the attenuation level ΔTL within a specific frequency range. The frequencies f_{L} and f_{U} are set to 550 Hz and 750 Hz, respectively, with a minimum bandwidth Δf of approximately 100 Hz. The penalty factor ζ is reduced to 0.2, reducing the weight of the second term in the objective function. Results, shown in Figure 4(b), indicate an increase in attenuation level with more resonating layers. Unlike the previous scenario, the optimization strategy consistently finds n-MLAM configurations that enhance attenuation compared to the n-layered homogeneous material. Specifically, n-MLAM panels with 2, 3, and 4 resonating layers achieve attenuation levels of 28 dB, 34 dB, and 44 dB, respectively. This increase is achieved while maintaining a constant surface density and a minimum bandwidth of approximately 100 Hz, highlighting the advantage of more resonators.

5 CONCLUSIONS

This study demonstrates the benefits of enhancing sound transmission loss (STL) by coupling multiple peaks through local resonance effects. Combining conventional acoustic metamaterial structures with compliant mechanisms improves STL, extending attenuation bandwidth to lower frequencies and increasing attenuation levels. However, it also requires more stringent stiffness properties, potentially needing softer materials or increased panel thickness.

The proposed n-MLAM panel design effectively realizes multiple coupled resonances with a layered structure suitable for large-scale manufacturing. Computational homogenization and machine learning techniques enhance the design strategy, making the optimization process more efficient and broadening the range of potential solutions. n-MLAM panels offer a promising approach to address challenges in existing acoustic metamaterial technologies for sound insulation applications.

REFERENCES

[1] Z. Liu, X. Zhang, Y. Mao, Y. Zhu, Z. Yang, C. T. Chan, and P. Sheng. Locally Resonant Sonic Materials. *Science*, 289(5485):1734–1736, sep 2000.

[2] Mahmoud I Hussein, Michael J Leamy, and Massimo Ruzzene. Dynamics of phononic materials and structures: Historical origins, recent progress, and future outlook. *Applied Mechanics Reviews*, 66(4), 2014.

[3] Yan Pennec, Bahram Djafari-Rouhani, H Larabi, JO Vasseur, and AC Hladky-Hennion. Low-frequency gaps in a phononic crystal constituted of cylindrical dots deposited on a thin homogeneous plate. *Physical Review B*, 78(10):104105, 2008.

[4] David Roca and Mahmoud I Hussein. Broadband and intense sound transmission loss by a coupled-resonance acoustic metamaterial. *Physical Review Applied*, 16(5):054018, 2021.

[5] A Stein, M Nouh, and T Singh. Widening, transition and coalescence of local resonance band gaps in multi-resonator acoustic metamaterials: From unit cells to finite chains. *Journal of Sound and Vibration*, 523:116716, 2022.

[6] Xiaopeng Wang, Yongyong Chen, Guojian Zhou, Tianning Chen, and Fuyin Ma. Synergetic coupling large-scale plate-type acoustic metamaterial panel for broadband sound insulation. *Journal of Sound and Vibration*, 459:114867, 2019.

[7] D. Roca, J. Cante, O. Lloberas-Valls, T. Pàmies, and J. Oliver. Multiresonant layered acoustic metamaterial (mlam) solution for broadband low-frequency noise attenuation through double-peak sound transmission loss response. *Extreme Mechanics Letters*, 47:101368, 2021.

[8] G. Sal-Anglada, D. Yago, J. Cante, J. Oliver, and D. Roca. Sound transmission loss enhancement through triple-peak coupled resonances acoustic metamaterials. *International Journal of Mechanical Sciences*, 266:108951, 2024.

[9] G. Sal-Anglada, D. Yago, J. Cante, J. Oliver, and D. Roca. Optimal design of multiresonant layered acoustic metamaterials (mlam) via a homogenization approach. *Engineering Structures*, 293:116555, 2023.

[10] D. Yago, G. Sal-Anglada, D. Roca, J. Cante, and J. Oliver. Machine learning in solid mechanics: Application to acoustic metamaterial design. *International Journal for Numerical Methods in Engineering*, page e7476, 2024.

[11] Muhammad, John Kennedy, and C.W. Lim. Machine learning and deep learning in phononic crystals and metamaterials – a review. *Materials Today Communications*, 33:104606, 2022.

[12] D. Roca, O. Lloberas-Valls, J. Cante, and J. Oliver. A computational multiscale homogenization framework accounting for inertial effects: Application to acoustic metamaterials modelling. *Computer Methods in Applied Mechanics and Engineering*, 330:415–446, mar 2018.